1971Ap&SS..14..399E

THE EVOLUTION OF HYDROGEN-HELIUM STARS

DILHAN EZER
Goddard Institute for Space Studies, NASA, New York, U.S.A.

and

A. G. W. CAMERON
Belfer Graduate School of Science, Yeshiva University, New York, N.Y., U.S.A.
and
Goddard Institute for Space Studies, NASA, New York, N.Y., U.S.A.

(Received 10 May, 1971; in revised form 21 July, 1971)

Abstract. According to the work of Truran and Cameron, and of others, on the chemical evolution of the Galaxy, the first generation of stars in the Galaxy contained principally massive objects. If big-bang nucleosynthesis was responsible for the formation of helium, the the first generation of stars would contain about 80 % hydrogen and 20 % helium, to be consistent with the approximately 22 % helium found in recent stellar evolutionary studies of the Sun. The present investigation has followed the pre-main sequence evolution and the main sequence evolution of stars of 5, 10, 20, 30, 100, and 200 $M_{\odot}$. Normal stars in this entire mass range normally convert hydrogen into helium by the CN-cycle on the main sequence. The present hydrogen-helium stars of 5 and 10 $M_{\odot}$ must reach higher central temperatures in order to convert hydrogen to helium by the proton-proton chains. Consequently, the mean densities in the stars are greater, and the surface temperatures are higher than in normal stars. In the stars of 20 $M_{\odot}$ and larger, the proton-proton chains do not succeed in supplying the necessary luminosity of the stars by the time the contraction has produced a central temperature near 10^8 K. At that point triple-alpha reactions generate small amounts of C^{12}, which then acts as a catalyst in the CN-cycle, the rate of which is then limited by the beta-decays occurring within the cycle. During the evolution of these more massive stars, the central temperature remains in the vicinity of 10^8 K, and the surface temperature on the main sequence approaches 10^5 K. The star of 200 $M_{\odot}$ becomes unstable against surface mass loss through radiation pressure in the later stages of its main sequence evolution, and these mass loss effects were not followed. Young galaxies containing these massive stars will have a very high luminosity, but if they have formed at one-tenth the present age of the universe or later, then the light from them will mainly reside in the visible or ultraviolet, rather than in the infrared as has been suggested by Partridge and Peebles.

1. Introduction

If current ideas concerning nucleosynthesis in stars are correct, then the first generation of stars to be formed is likely to contain only hydrogen and helium, and no heavier elements. There is still considerable discussion about the expected helium content of the early galaxy, but most studies of stellar evolution are consistent with a large initial helium content, and as yet no convincing way has been shown of forming large amounts of helium through stellar processes in the early history of the galaxy. Furthermore, owing to the extreme scarcity of very old stars of slightly less than 1 solar mass with extreme deficiencies of the metals, Schmidt (1963) and Truran and Cameron (1971) have argued that the earliest stars to be formed in a galaxy, which will be responsible for the early manufacture of the metals, must all be massive ones. This has provided the motivation for the present study of the structure and evolution of massive hydrogen-helium stars.

Astrophysics and Space Science **14** (1971) 399–421. *All Rights Reserved*
Copyright © 1971 by D. Reidel Publishing Company, Dordrecht-Holland

© Kluwer Academic Publishers • Provided by the NASA Astrophysics Data System

1971Ap&SS..14..399E

In a recent study of solar evolution (Ezer and Cameron, 1971), we have found that the present characteristics of the Sun can be well-represented with a helium abundance of 0.223. The absolute value of this helium abundance may be in error due to compensating errors in such physical quantities as the opacity, but to facilitate comparison of our hydrogen-helium models with normal stars, we have taken the above value as a basis for adjustment of the helium content of the hydrogen-helium stars. Since Truran and Cameron (1971) have found that only about 2% of the interstellar hydrogen has been converted to helium through stellar evolution by the time of formation of the sun, we have therefore chosen the composition of our hydrogen-helium stars to be 80% hydrogen and 20% helium. Opacity tables for the present study have been computed on the basis of this composition.

In this work the structure and evolution of hydrogen-helium stars of 5, 10, 20, 30, 100, and 200 $M_{\odot}$ have been followed through the pre-main sequence phases of evolution and through hydrogen-burning on the main sequence.

2. Computational Procedure

The method of computation was that used in our recent study (Ezer and Cameron, 1971), except that no mass loss effect has been considered in the present study. Initial models corresponding to the evolution time $t=0$ were taken at the threshold of energy stability (Ezer and Cameron, 1967). The number of models calculated in each evolutionary study varied between 70 and 250. The number of mass zones in any one model lay in the range 160 to 450. The program automatically inserted or deleted mass zones whenever changes in the physical variables became larger than the desired values.

The opacity for the hydrogen-helium mixture under study was obtained from the Cox opacity code. The opacity code was run for three mixtures in which the hydrogen-to-helium ratio was 4, 1, and 0. These three opacity tables were stored in the computer for temperature-density combinations characteristic of the structure of the stars. The required opacity of the material was obtained by interpolation between these tables.

The energy sources included in the study of the structure and evolution of the hydrogen-helium stars were gravitational contraction, the proton-proton chain, the carbon cycle, and the triple-alpha reaction. The nuclear parameters used for the second and third reactions are the same as in our recent work (Ezer and Cameron, 1971). It was assumed that, under conditions existing in the interiors of these stars, the equilibrium value of He^3 is easily maintained, and only the energy generation by the full proton-proton chain was considered.

The carbon cycle will become operative if a sufficient amount of carbon can be formed by the triple-alpha reaction. This reaction requires high temperatures to operate. Under ordinary circumstances the rate of the CN-cycle is basically determined by the rate of the N^{14} (p, γ) O^{15} reaction. But at temperatures around 10^8 K, the carbon cycle turn-over rate is governed by the beta-decay half-lives, and the most abundant nuclei are N^{13} and O^{15}. The lifetime of a C^{12} nucleus against proton capture, relative to the lifetime of a N^{14} nucleus against proton capture, becomes larger. We

© Kluwer Academic Publishers • Provided by the NASA Astrophysics Data System

1971Ap&SS..14..399E

have assumed that the steady-state abundance of C^{12} relative to N^{14} is maintained at lower temperatures in such a way that 75% of C^{12} formed by the triple-alpha reaction would be in the form of N^{14} thereafter.

Helium burning is limited to the triple-alpha reaction. The rate of destruction of He^4 per alpha particle per second is given (Reeves, 1965) by

$$\frac{P_\alpha}{(\varrho x_4)^2 f_{3\alpha}} = \frac{5.92 \times 10^{-7}}{T_8^3} \times 10^{-18.9/T_8}$$

The electron screening factor for the triple-alpha reaction, $f_{3\alpha}$ never departs much from unity under the conditions of interest in this paper, and weak screening expressions have been used.

During the evolutionary study, the changes in the abundances of hydrogen and helium, and the rate of C^{12} formation, were followed explicitly.

3. Overall Results of the Computations

The results of the computation for each mass have been plotted in the theoretical Hertzsprung-Russell diagram in Figure 1. The dots at the starting point of each evolutionary track are the positions of the stars of the indicated mass at an evolution time

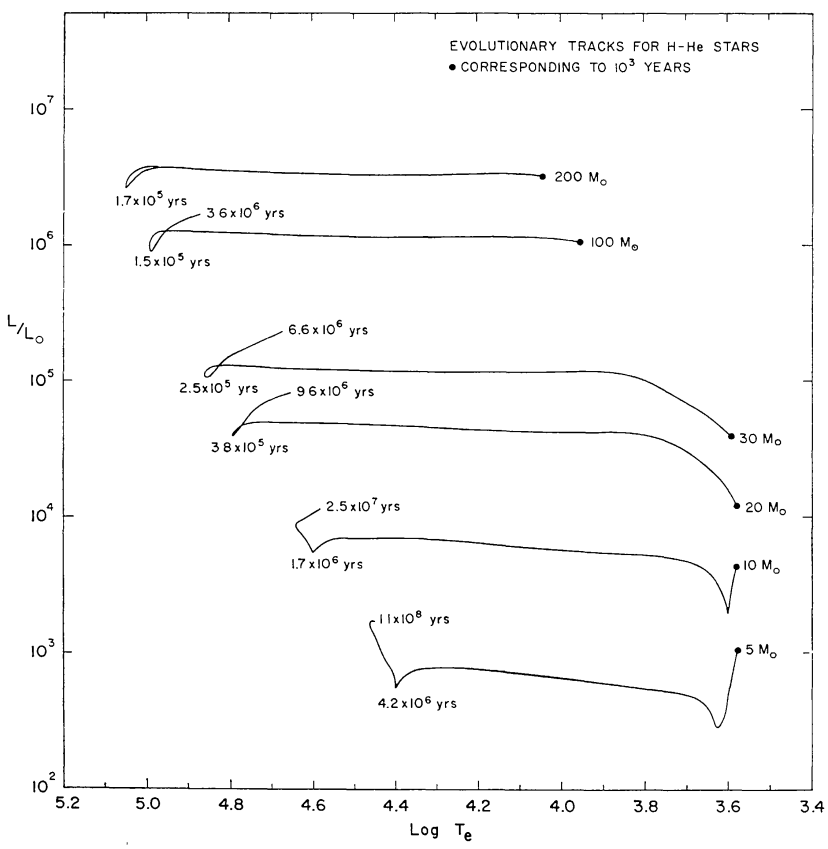

Fig. 1. The theoretical Hertzsprung-Russell diagram for hydrogen-helium stars of different masses.

© Kluwer Academic Publishers • Provided by the NASA Astrophysics Data System

1971Ap&SS..14..399E

of 10^3 yr, taking this time as zero at the threshold of stability. The zero-age main-sequence times, defined as the point at which the luminosity reaches its minimum value before the hydrogen-burning phase, are given in the figure. In each case, the evolutionary path has been indicated up to the point at which the hydrogen at the center of the star has almost been depleted, and the corresponding evolution time is shown. The last point in the evolutionary track of the 200 $M_\odot$ star corresponds to the model in which the central hydrogen content has been reduced from its initial value of 0.80 to 0.38. The physical characteristics of the models for the 5, 10, 20, 30, 100, and 200 $M_\odot$ are summarized in Table I, at the zero-age main-sequence, and in Table II at the end of the hydrogen-depletion phase. In each table, the first and second columns give the mass in solar units, and the zero-age main-sequence time in years. The third, fourth and fifth columns give the radius, luminosity in solar units and corresponding effective temperature. The sixth and seventh columns are the central temperature and central density; the eighth and ninth columns give the mass fraction of the convective core and the ratio of the gas pressure to the total pressure, β, at the center of the star.

In Table II, the last column indicates the amount of hydrogen remaining at the center of the stars.

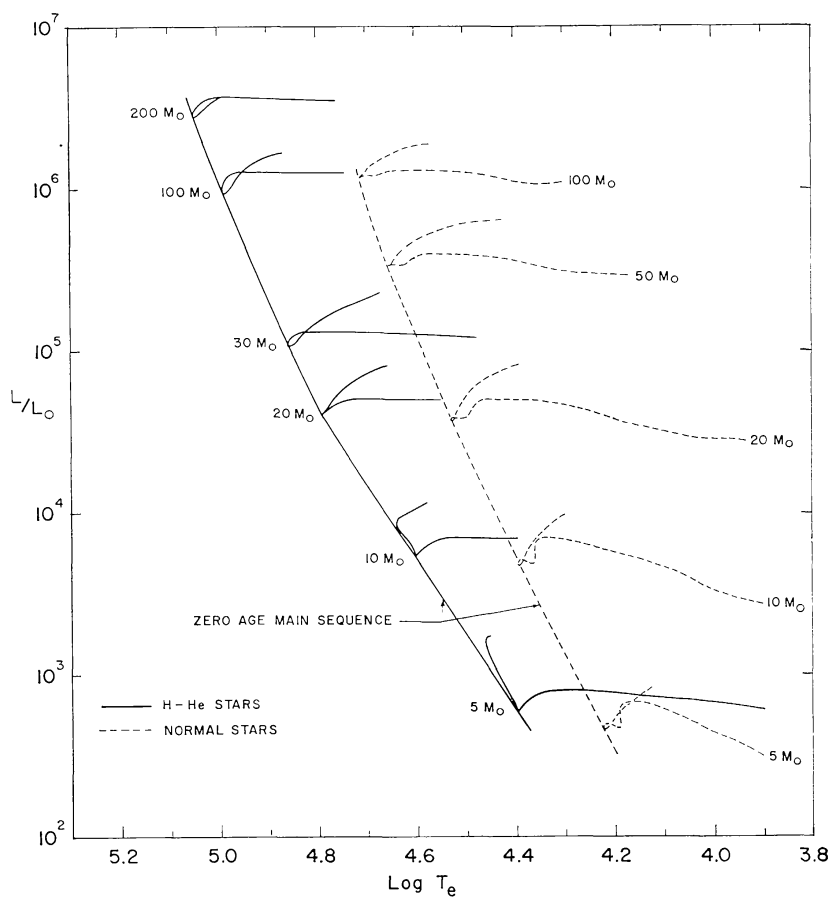

Fig. 2. The comparison of the evolutionary tracks of the hydrogen-helium stars of indicated masses with those of normal stars, in the H-R diagram.

© Kluwer Academic Publishers • Provided by the NASA Astrophysics Data System

1971Ap&SS..14..399E

TABLE I
The physical characteristics of the models at the zero-age main-sequence

$M/M_\odot$	t_{zams} yr	$R/R_\odot$	$L/L_\odot$	$\log T_e$	T_cK	ϱ_c g cm^{-3}	M_c/M	β_c
5	4.24×10^6	1.33	5.66×10^2	4.39	4.07×10^7	8.54×10	0.10	0.97
10	1.68×10^6	1.54	5.47×10^3	4.60	6.62×10^7	1.03×10^2	0.12	0.95
20	3.81×10^5	1.76	4.00×10^4	4.79	1.03×10^8	1.30×10^2	0.31	0.87
30	2.50×10^5	2.11	1.07×10^5	4.86	1.14×10^8	1.05×10^2	0.51	0.80
100	1.46×10^5	3.38	9.04×10^5	4.99	1.25×10^8	1.88×10	0.72	0.36
200	1.71×10^5	4.33	2.58×10^6	5.05	1.28×10^8	1.19×10	0.81	0.24

TABLE II
The physical characteristics of the models at the end of hydrogen-depletion phase

$M/M_\odot$	t yr	$R/R_\odot$	$L/L_\odot$	$\log T_e$	T_cK	ϱ_c g cm^{-3}	M_c/M	β_c	X_{1c}
5	1.09×10^8	1.77	1.76×10^3	4.45	9.37×10^7	8.24×10^2	0.05	0.96	0.010
10	2.54×10^7	2.49	1.17×10^4	4.58	1.05×10^8	3.08×10^2	0.11	0.87	0.010
20	9.60×10^6	4.68	8.64×10^4	4.66	1.25×10^8	1.86×10^2	0.20	0.70	0.003
30	6.61×10^6	7.02	2.34×10^5	4.68	1.33×10^8	1.41×10^2	0.27	0.60	0.003
100	3.64×10^6	7.76	1.70×10^6	4.78	1.36×10^8	2.15×10	0.38	0.18	0.007

© Kluwer Academic Publishers • Provided by the NASA Astrophysics Data System

1971Ap&SS..14..399E

In Figure 2, the evolutionary tracks of the hydrogen-helium stars of indicated mass have been compared with those of normal stars in the H-R diagram. The zero-age main-sequence positions of these stars occur at effective temperatures higher than those of normal stars by values ranging between 0.15 and 0.27 in log T_e. In Table III, the zero-age main-sequence time and surface characteristics of hydrogen-helium stars of 5, 10, 20, and 100 $M_\odot$ are compared with those of normal stars with the same mass. The symbols in the table have their usual meanings. The zero-age main-sequence times of these stars are longer than those of normal stars. In Table IV, the central characteristics of the hydrogen-depleted models are given for these stars and for normal stars with an initial hydrogen content 0.739. The columns from one to four are self-explanatory. The values in the column X_{1c} show the central hydrogen content, and those in the column M_c/M give the fractional mass inside the main convective core. The stars with mass equal to or larger than 10 $M_\odot$ all have semi-convective regions besides the main convective core.

Figure 3 shows the central temperatures and densities of hydrogen-helium stars of indicated mass and those of normal stars. The heavy lines correspond to the values at the zero-age main-sequence, and the light ones to those at the end of the hydrogen-depletion phase. For hydrogen-helium stars of mass greater than 20 $M_\odot$, the central temperature on the main-sequence exceeded 10^8 K, so that helium-burning produced sufficient carbon for the operation of carbon cycle in the interior. For pure hydrogen

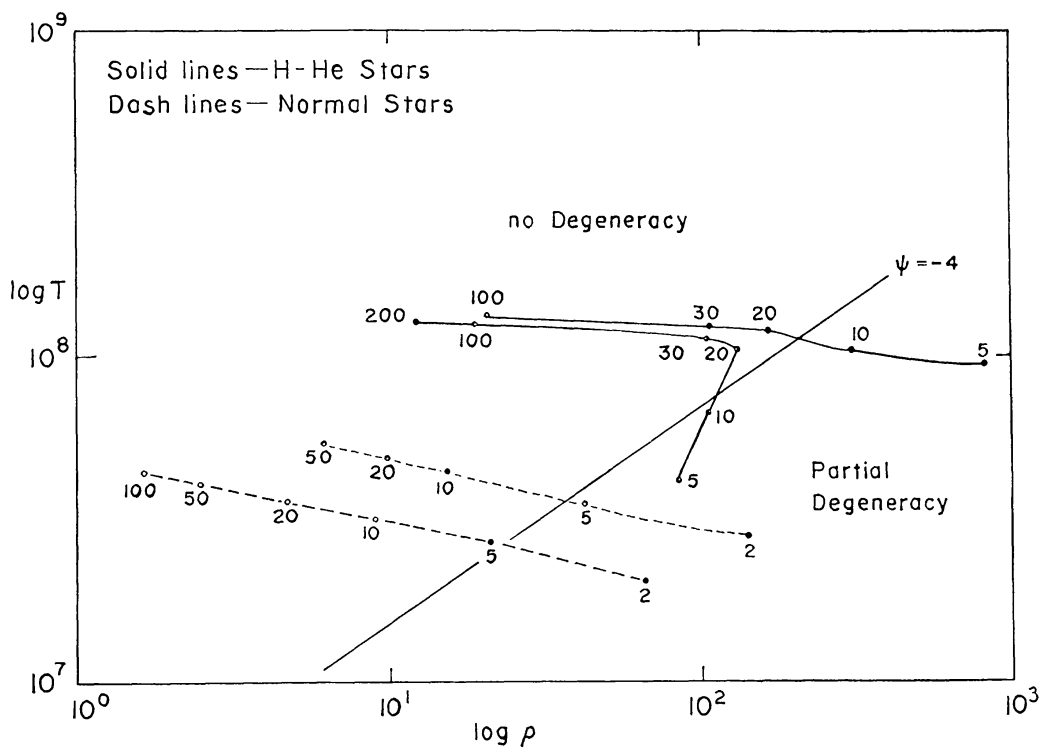

Fig. 3. The central temperatures and densities of the hydrogen-helium stars of indicated masses and those of normal stars.

© Kluwer Academic Publishers • Provided by the NASA Astrophysics Data System

1971Ap&SS..14..399E

TABLE III
Zero-age main-sequence time and surface characteristics

	H-He stars				Normal stars			
$M/M_\odot$	Time yr	$L/L_\odot$	$R/R_\odot$	log T_e	Time yr	$L/L_\odot$	$R/R_\odot$	logT_e
5	4.24×10^6	5.66×10^2	1.33	4.39	1.49×10^6	4.48×10^2	2.55	4.22
10	1.68×10^6	5.47×10^3	1.54	4.60	3.84×10^5	4.66×10^3	3.84	4.39
20	3.81×10^5	4.00×10^4	1.76	4.79	1.67×10^5	3.67×10^4	5.71	4.53
100	1.46×10^5	9.04×10^5	3.38	4.99	1.93×10^4	1.18×10^6	13.50	4.72

TABLE IV
Central characteristics of hydrogen-depleted models Δt = hydrogen depletion time

	H-HE stars $X_{\text{initial}} = 0.80$					Normal stars $X_{\text{initial}} = 0.739$				
$M/M_\odot$	Δt yr	T_cK	ϱ_c g cm^{-3}	X_{1c}	M_c/M	Δt yr	T_cK	ϱ_c g cm^{-3}	X_{1c}	M_c/M
5	1.0×10^8	9.37×10^7	8.24×10^2	0.010	0.05	9.8×10^7	3.52×10^7	4.12×10	0.011	0.08
10	2.4×10^7	1.05×10^8	3.08×10^2	0.010	0.11	2.6×10^7	4.68×10^7	2.02×10	0.006	0.14
20	9.2×10^6	1.25×10^8	1.86×10^2	0.003	0.20	9.8×10^6	4.79×10^7	9.78	0.008	0.25
100	2.8×10^6	1.18×10^8	1.34×10	0.243	0.49	2.7×10^6	4.50×10^7	1.74	0.248	0.60

© Kluwer Academic Publishers • Provided by the NASA Astrophysics Data System

1971Ap&SS..14..399E

stars, this mass limit has been found to be 26 $M_\odot$ (Ezer, 1961). The presence of 20% helium in the initial composition brings the limit down to 20 $M_\odot$.

In Figure 4, the variations, within the stars of indicated masses, of the fractional mass inside the convective core (M_c/M), the central ratio of the gas pressure to the total pressure (β), and of the relative contribution of the rate of energy generation by the p-p chain reactions ($\varepsilon_{pp}/\varepsilon_{NT}$), and CN-cycle reaction ($\varepsilon_{CN}/\varepsilon_{NT}$) to the total rate of nuclear energy generation at the center of the stars, are shown for the zero-age main-sequence models. The 5 and 10 $M_\odot$ stars derive their nuclear energy entirely from the p-p chain reactions. For the 20 $M_\odot$ star, only four percent of the total nuclear energy is due to the CN-cycle reactions; the rest is supplied by the p-p chain reactions. For the 30 $M_\odot$ star about 25% of the total nuclear energy is provided by the p-p chain reactions and 75% by the CN-cycle reactions. In the case of the 100 and 200 $M_\odot$ stars, the nuclear energy generation is almost entirely via the CN-cycle reactions.

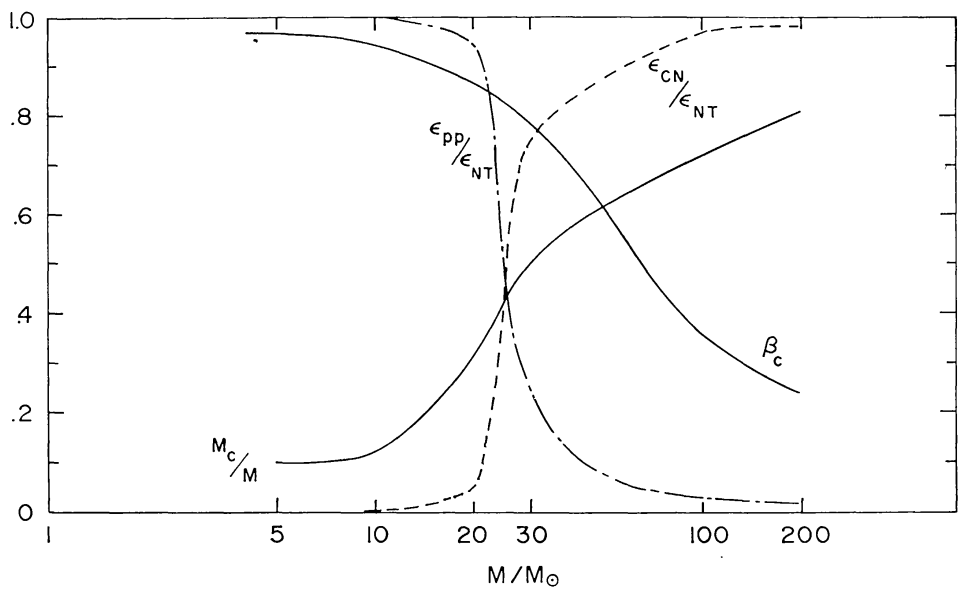

Fig. 4. The variation, with the stars of indicated masses, of the fractional mass inside the convective core (M_c/M), the central ratio of the gas pressure to the total pressure (β), the relative contribution of the rate of energy generation by the *p-p* chain reactions ($\varepsilon_{pp}/\varepsilon_{NT}$), and by the CN-cycle reactions ($\varepsilon_{CN}/\varepsilon_{NT}$) to the total rate of nuclear energy generation at the center of the star for the zero-age main-sequence models.

4. Evolution of 5 $M_\odot$ and 10 $M_\odot$ Stars

The evolutionary tracks for these stars are shown in the theoretical H-R diagram in Figure 1. The pre-main sequence evolution of these stars is similar to that of normal stars. But the time during which they stay fully convective is much shorter. The low opacity of the material with no heavy elements favors the development of a radiative core at lower temperatures through a rapid decrease of the temperature gradient. The luminosity decreases until a large part of the stellar mass becomes radiative, but it remains higher than that of normal stars. The increase in luminosity during the approach

© Kluwer Academic Publishers • Provided by the NASA Astrophysics Data System

1971Ap&SS..14..399E

to the main-sequence is not so pronounced. The main difference of the evolution is on the approach to the main sequence and during the main-sequence phases as seen in Figure 2. In the evolution of normal massive stars, when the purely gravitational contraction phase is completed, energy generation by nuclear burning begins to contribute to the total energy output of the star, and hence a moderate increase in the luminosity of the star takes place. This nuclear energy generation is mostly due to C^{12} depletion; when a steady-state equilibrium with N^{14} occurs, the full CN-cycle becomes operative.

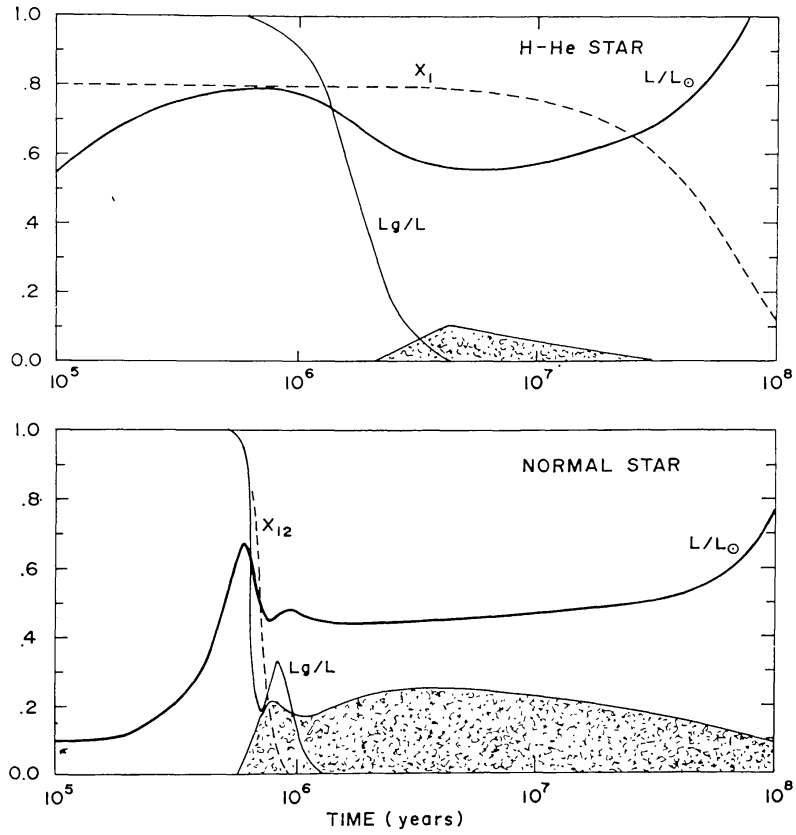

Fig. 5. The variation, with time, of some of the physical and compositional variables of the 5 $M_\odot$ star. The upper portion of the figure is for the hydrogen-helium star; the lower one is for a normal star.

In Figure 5, some of the details of the evolution of a 5 $M_\odot$ star are presented; the lower part shows the evolution of a normal star and the upper part that of a H-He star. L and L_g/L represent the variation with time of the total luminosity in solar units and the relative contribution of the gravitational contraction energy to the total luminosity, respectively. The curves X_{12} in the bottom figure and X_1 in the upper figure give the variation with time of the abundances of C^{12} and H at the center of the star. The mass fraction inside the convective core is also indicated by shading the figure. While C^{12} is being burned, the nuclear energy released supplements the contribution of the gravitational contraction to the total energy output; hence the luminosity shows an increase during the evolution of a normal star. The sudden development of the convec-

© Kluwer Academic Publishers • Provided by the NASA Astrophysics Data System

1971Ap&SS..14..399E

tive core at the center, due to nuclear burning, reduces the gravitational contraction energy of the star and absorbs some of the nuclear energy produced, so that the luminosity declines. Once C^{12} has been substantially converted to N^{14}, the central region contracts with a net rate of release of gravitational energy, and there is a second moderate increase in the luminosity. The rising interior temperature and density concentrates the nuclear sources near the center, and again the boundary of the central convective region extends to a larger mass fraction. Finally, gravitational energy release vanishes and the luminosity drops to its zero-age main-sequence value. These features of the evolution of normal stars were discussed by Iben (1965) and Ezer and Cameron (1967).

In the evolution of H-He stars, toward the end of the purely gravitational contraction phase, p-p chain reactions start to supplement the gravitational contraction energy. The p-p chain has a low temperature dependence. As the nuclear burning gradually takes over the total energy output of the star, the luminosity shows a moderate decline. The 5 $M_\odot$ and 10 $M_\odot$ stars reach the zero-age main-sequence in 4.24×10^6 and 1.68×10^6 yr, respectively. The zero-age main-sequence radius of the H-He star of 5 $M_\odot$ is 1.33 $R_\odot$ and that of the 10 $M_\odot$ is 1.54 $R_\odot$. These values are less than half of the zero-age main-sequence radii of normal stars with the same mass. Hence the surface temperatures of the stars are higher. At the center of the stars partial degeneracy of electrons occurs. The increases in central temperature and density are not quite proportional to $T_c \sim R^{-1}$ and $\varrho_c \sim R^{-3}$, since the degeneracy provides part of the support in the interior layers of the stars. Low temperature-sensitive p-p chain reactions produce only a small convective core at the center; the size of the convective core at the zero-age main-sequence is 0.10 and 0.12 of the total mass for the 5 $M_\odot$ and 10 $M_\odot$ stars, respectively. The central convective core disappears when the central hydrogen content has dropped to 0.60 for the 5 $M_\odot$ star and to 0.48 for the 10 $M_\odot$ star. The distribution of physical and compositional parameters versus mass fraction are given in Table Va for the 5 $M_\odot$ and in Table VIa for the 10 $M_\odot$ stars at the zero-age main-sequence. The first column gives the fractional mass of the star. The other columns give, in turn, the radius (cm), density (g cm^{-3}), temperature (°K) and luminosity (erg s^{-1}), at the selected mass fractions, X_1, X_4 and X_{12} are the abundances, by mass, of hydrogen, helium and carbon, ε_{pp} is the rate of energy production per gram per second by the p-p clain, ε_{CN} by the CN-cyle and $\varepsilon_{3\alpha}$ by the triple-alpha reaction. The last column, β, is the ratio of the gas pressure to the total pressure.

Unlike the situation in normal stars, two-thirds of the hydrogen-burning in the 5 $M_\odot$ star and more than half of the hydrogen-burning in the 10 $M_\odot$ star occurs in the radiative part of the core. This prevents the formation of a large discontinuity in composition in the interior of the star. Hydrogen-burning occurs in a larger fraction of the stellar mass. Due to this condition and the partial degeneracy of the interior, the central contraction is very slow during the last part of the hydrogen depletion phase. The surface layers expand only slightly, and the evolutionary track moves along the main-sequence as shown in Figure 2, until the hydrogen content at the center has dropped to 0.07 in the 5 $M_\odot$ star and to 0.37 in the 10 $M_\odot$ star. By that time, the central

© Kluwer Academic Publishers • Provided by the NASA Astrophysics Data System

1971Ap&SS..14..399E

temperatures and densities have risen to 8×10^7 K, 9×10^7 K and 1.28×10^3 g cm^{-3}, 2.70×10^2 g cm^{-3} for 5 $M_\odot$ and 10 $M_\odot$ stars, respectively. Even though the fractional carbon abundance is quite small (8.8×10^{-11} for 5 $M_\odot$ and 9.4^{-11} for 10 $M_\odot$), the continued operation of the triple-alpha reaction in the core makes the contribution to energy generation from the CN-cycle become progressively more important. This again causes the development of a central convective core, but this never exceeds 0.5% of the total mass of the 5 $M_\odot$ star. Since at this time the hydrogen content has been depleted to 0.07 at the center, the development of the small convective core causes only a small discontinuity in composition. The turn-off from the main sequence occurs at this point, accompanied by a moderate increase in the radius. When the hydrogen abundance at the center has dropped to 0.01, the energy generation is almost entirely via the CN-cycle reactions over 10% of the stellar mass, and the p-p chain reactions occur throughout roughly 70% of the stellar mass.

In the evolution of the 10 $M_\odot$ star, the CN-cycle reactions extend the boundary of the second convective core up to a fractional mass 0.19 when the central hydrogen has fallen to 0.26. The extension of the convective core prevents a rapid increase of the energy generation by the CN-cycle by reducing the C^{12} at the center of the star. However, there is not a sharp discontinuity in the hydrogen profile, since the p-p chain reactions operate throughout a large extent of the stellar mass. When the central hydrogen abundance drops to 0.01, the energy generation by the CN-cycle exceeds that of the p-p chain reactions inside 15% of the stellar mass, and the p-p chain reactions operate throughout an additional 65% of the stellar mass.

In Table Vb and VIb, the physical and compositional characteristics have been summarized for the models corresponding to the end of the hydrogen depletion phase, for the 5 $M_\odot$ and 10 $M_\odot$ stars, respectively. The columns correspond to those in Tables Va and VIa.

5. Evolution of More Massive Stars

The theoretical evolutionary tracks for stars of 20 $M_\odot$, 30 $M_\odot$, 100 $M_\odot$, and 200 $M_\odot$ in the H-R diagram are also shown in Figure 1.

The evolution of these stars until the completion of the purely gravitational contraction phase is not very different from the evolution of normal stars. The luminosities are comparable to those of normal stars since the opacity is mostly due to electron scattering. In the evolution of a normal star with a mass of 20 $M_\odot$, when it contracts to a radius of 12 $R_\odot$ with a luminosity of 5×10^4 $L_\odot$, the central temperature and density have risen to about 20×10^6 K and 1 g cm^{-3}, respectively. At this temperature and density, energy generation by C^{12} depletion is the main contributor to the energy production. This will cause a moderate increase in the luminosity of the star. Even though the C^{12} depletion time is quite short, the development of the convective core reduces the contribution of gravitational energy to the total energy output of the star, and hence causes a decline in the luminosity. This produces the first minimum value in luminosity, before it drops down its lowest zero-age main-sequence value. As the

© Kluwer Academic Publishers • Provided by the NASA Astrophysics Data System

1971Ap&SS..14..399E

TABLE Va

Zero-age main-sequence model for $M = 5\ M_\odot$ $t_{\text{zams}} = 4.23 \times 10^6$ yr

M_r/M	R cm	ϱ g cm^{-3}	T K	L erg s^{-1}	X_1	X_4	X_{12}	ε_{pp} erg cm^{-1} s^{-1}	ε_{CN} erg g^{-1} s^{-1}	$\varepsilon_{3\alpha}$ erg g^{-1} s^{-1}	β
0.00	0.00	8.54×10^1	4.07×10^7	0.00	0.789	0.211		1.63×10^3			0.97
0.05	1.15×10^{10}	7.26	3.68	5.96×10^{35}	0.789	0.211		1.04×10^3			0.97
0.10	1.48	6.53	3.43	1.03×10^{36}	0.789	0.211		7.63×10^2			0.99
0.15	1.78	5.90	3.23	1.35	0.794	0.206		5.79			0.99
0.20	1.94	5.33	3.04	1.60	0.796	0.204		4.28			0.99
0.30	2.30	4.37	2.71	1.91	0.797	0.203		2.29			0.99
0.40	2.63	3.56	2.51	2.08	0.798	0.202		1.10			0.99
0.50	2.96	2.73	2.18	2.15	0.799	0.201		4.67×10^1			0.99
0.60	3.30	2.00	1.91	2.18	0.799	0.201		1.80			0.99
0.70	3.68	1.41	1.66	2.19	0.799	0.201		6.83×10^0			0.99
0.80	4.17	7.77×10^0	1.36	2.20	0.800	0.200					0.99
0.90	4.85	3.67	1.03	2.20	0.800	0.200					0.99
0.95	5.44	1.70	7.90×10^6	2.21	0.800	0.200					0.99
1.00	9.24×10^{10}	3.59×10^{-9}	2.45×10^4	2.21×10^{36}	0.800	0.200					0.93

TABLE Vb

Hydrogen-depleted model for $M = 5\ M_\odot$ $t = 1.09 \times 10^8$ yr

M_r/M	R cm	ϱ g cm^{-3}	T K	L erg s^{-1}	X_1	X_4	X_{12}	ε_{pp} erg c^{-1} s^{-1}	ε_{CN} erg g^{-1} s^{-1}	$\varepsilon_{3\alpha}$ erg g^{-1} s^{-1}	β
0.00	0.00	8.24×10^2	9.37×10^7	0.00	0.011	0.989	2.82×10^{-9}	2.25×10^1	2.05×10^4	3.93×10^{-3}	0.96
0.05	5.63×10^9	5.73	7.56	2.78×10^{36}	0.011	0.989	2.82	1.01	1.39×10^3	5.30×10^{-8}	0.97
0.10	7.73	3.39	6.53	3.36	0.182	0.818	8.91×10^{-15}	1.15×10^3	2.23×10^{-3}		0.98
0.15	9.57	2.36	5.85	3.95	0.263	0.737		1.25	2.61×10^{-5}		0.98
0.20	1.14×10^{10}	1.66	5.31	4.51	0.353	0.647		1.22			0.98
0.30	1.51	8.76×10^1	4.44	5.65	0.521	0.479		9.13×10^2			0.98
0.40	1.93	4.95	3.70	6.35	0.653	0.347		4.96			0.98
0.50	2.37	3.01	3.09	6.70	0.734	0.266		2.20			0.98
0.60	2.87	1.85	2.57	6.83	0.775	0.225		7.22×10^1			0.98
0.70	3.41	1.11	2.12	6.87	0.793	0.207		1.66			0.98
0.80	4.16	5.53×10^0	1.65	6.88	0.798	0.202		2.67×10^0			0.99
0.90	5.19	2.08	1.16	6.88	0.800	0.200					0.99
0.95	6.06	8.92×10^{-1}	8.81×10^6	6.88	0.800	0.200					0.99
1.00	1.23×10^{11}	2.62×10^{-9}	2.82×10^4	6.88×10^{36}	0.800	0.200					0.87

© Kluwer Academic Publishers • Provided by the NASA Astrophysics Data System

1971Ap&SS..14..399E

TABLE VIa

Zero-age main-sequence model for $M = 10\ M_\odot$ $t_{\text{zams}} = 1.68 \times 10^6$ yr

M_r/M	R cm	ϱ g cm^{-3}	T K	L erg s^{-1}	X_1	X_4	X_{12}	ε_{pp} erg cm^{-1} s^{-1}	ε_{CN} erg g^{-1} s^{-1}	$\varepsilon_{3\alpha}$ erg g^{-1} s^{-1}	β
0.00	0.00	1.03×10^2	6.62×10^7	0.00	0.783	0.217		6.40×10^3			0.95
0.05	1.38×10^{10}	8.70×10^1	5.98	5.07×10^{36}	0.783	0.217		4.30			0.96
0.10	1.75	7.84	5.64	8.54	0.783	0.217		3.36			0.96
0.15	2.05	7.06	5.32	1.14×10^{37}	0.789	0.211		2.67			0.96
0.20	2.31	6.36	5.02	1.38	0.792	0.208		2.10			0.97
0.30	2.74	5.18	4.52	1.70	0.795	0.205		1.31			0.97
0.40	3.15	4.09	4.03	1.91	0.797	0.203		7.69×10^2			0.97
0.50	3.52	3.21	3.61	2.02	0.798	0.202		4.44			0.98
0.60	3.93	2.39	3.17	2.09	0.799	0.201		2.20			0.98
0.70	4.38	1.67	2.74	2.12	0.799	0.201		9.3×10^1			0.98
0.80	4.95	9.90×10^0	2.26	2.13	0.800	0.200					0.98
0.90	5.76	4.43	1.71	2.13	0.800	0.200					0.98
0.95	6.43	2.12	1.33	2.13	0.800	0.200					0.98
1.00	1.07×10^{11}	4.12×10^{-9}	2.04×10^4	2.13×10^{37}	0.800	0.200					0.78

TABLE VIb

Hydrogen-depleted model for $M = 10\ M_\odot$ $t = 2.54 \times 10^7$ yr

M_r/M	R cm	ϱ g cm^{-3}	T K	L erg s^{-1}	X_1	X_4	X_{12}	ε_{pp} erg cm^{-1} s^{-1}	ε_{CN} erg g^{-1} s^{-1}	$\varepsilon_{3\alpha}$ erg g^{-1} s^{-1}	β
0.00	0.00	3.08×10^2	1.05×10^8	0.00	0.011	0.989	1.16×10^{-8}	9.68×10^0	9.61×10^4	5.96×10^{-2}	0.87
0.05	9.78×10^9	2.18	8.98×10^7	3.20×10^{37}	0.011	0.989	1.16	5.00	1.28	3.29×10^{-5}	0.88
0.10	1.28×10^{10}	1.71	7.88	3.87	0.011	0.989	1.16	3.00	2.55×10^3		0.90
0.15	1.61	9.57×10^1	6.87	4.06	0.224	0.776	1.00×10^{-10}	5.24×10^2	5.24×10^2		0.91
0.20	1.96	5.85	6.10	4.18	0.471	0.529		1.03×10^3	6.50×10^0		0.92
0.30	2.63	3.56	5.02	4.36	0.596	0.404		6.68×10^2			0.93
0.40	3.27	2.32	4.22	4.46	0.681	0.319		3.70			0.94
0.50	3.92	1.54	3.58	4.51	0.732	0.266		1.76			0.95
0.60	4.61	1.00	2.99	4.53	0.766	0.234		7.40×10^1			0.95
0.70	5.40	6.23×10^0	2.52	4.54	0.785	0.215		2.50			0.96
0.80	6.43	3.26	2.00	4.55	0.795	0.203		3.70×10^0			0.96
0.90	7.86	1.31	1.44	4.55	0.800	0.200					0.96
0.95	9.09	5.79×10^{-1}	1.09	4.55	0.800	0.200					0.96
1.00	1.73×10^{11}	2.14×10^{-9}	3.82×10^4	4.55×10^{37}	0.800	0.200					0.68

© Kluwer Academic Publishers • Provided by the NASA Astrophysics Data System

1971Ap&SS..14..399E

star contracts to half of the above radius, the full p-p chain and CN-cycle reactions have replaced gravitational contraction as the entire source of outgoing energy, and the luminosity achieves its final minimum value representing the zero-age main-sequence state in 1.7×10^5 yr. The surface temperature is then about 3.3×10^4 K.

In the evolution of H-He star of 20 $M_\odot$, toward the completion of the purely gravitational contraction phase, the contribution of the gravitational contraction energy greatly exceeds that from the p-p chain reactions, which have low temperature dependence. In order for the star to maintain its energy output, it must keep contracting, reducing its radius to about 2 $R_\odot$ near the zero-age main-sequence. Therefore, the zero-age main-sequence surface temperature is about twice as high as that of a normal 20 $M_\odot$ star. Because of the small temperature sensitivity of the p-p chains at these high temperatures, the energy generation is only moderately concentrated toward the center. The convective core covers about 31% of the total mass in the 20 $M_\odot$ star. The zero-age main-sequence time is 3.81×10^5 yr. The physical and compositional parameters of the zero-age main-sequence model of the 20 $M_\odot$ star are given in Table VIIa, which has a format identical to those of Table Va and VIa.

The main sequence evolution of this star depends on the central temperature that it attains at the zero-age main-sequence. A temperature of 1.03×10^8 K and a density of 1.3×10^2 g cm^{-3} are then reached at the center and the energy generation by the triple-alpha reaction becomes 4.12×10^{-5} erg g^{-1} s^{-1}. The fractional mass of carbon has reached 4.26×10^{-12}. The rate at which the carbon cycle turns over is governed by the beta-decay half-lives. The rate of energy generation by CN-cycle is 8.5×10^2 erg g^{-1}s^{-1}, which is still small compared to 2.03×10^4 erg g^{-1} s^{-1} generated by the p-p chain reactions.

After an evolution time of 1.6×10^8 yr, the rate of energy generation by the CN-cycle exceeds that by the p-p chain reactions. At this time the hydrogen abundance has dropped to 0.73 at the center and the fractional mass of carbon is 1.06×10^{-10}.

The main-sequence evolution depends on the conditions prevailing in the interior of the star. The central temperature should stay high enough so that carbon formation can continue at a very slow rate.

During the hydrogen depletion phase, the high value of the nuclear energy generation rate at the center favors the expansion of the central convective core and the reduction of the central temperature, T_c, and density, ϱ_c, slightly; but T_c never becomes less than 1.02×10^8 K. Meanwhile, the total luminosity increases and $L \sim \mu^4 M^{2.5}$ for an opacity due to electron scattering, with μ being the mean molecular weight. Once the conversion of hydrogen to helium sufficiently increases μ, the central temperature starts to increase. The total radius also increases. When the hydrogen content is reduced to 0.003 at the center of the star, the central temperature $T_c = 1.25 \times 10^8$ K and the central density $\varrho_c = 186$ g cm^{-3}, and $\beta_c = 0.70$. The high value of β still keeps quite a large part of the star convective ($M_c \sim 0.20\ M_T$). Within the central 30% of the stellar mass, the energy generation is mainly due to CN-cycle reactions. At the fractional mass 0.3, the temperature is 6.5×10^7 K and the density is 24 g cm^{-3}. The consumption of hydrogen will continue by the p-p chain reactions outside this point

© Kluwer Academic Publishers • Provided by the NASA Astrophysics Data System

1971Ap&SS..14..399E

TABLE VIIa
Zero-age main-sequence model for $M = 20\ M_\odot$ $t_{\text{zams}} = 3.81 \times 10^5$ yr

M_r/M	R cm	ϱ g cm^{-3}	T K	L erg s^{-1}	X_1	X_4	X_{12}	ε_{pp} erg cm^{-1} s^{-1}	ε_{CN} erg g^{-1} s^{-1}	$\varepsilon_{3\alpha}$ erg g^{-1} s^{-1}	β
0.00	0.00	1.30×10^2	1.03×10^8	0.00	0.789	0.211	4.26×10^{-12}	2.03×10^4	8.50×10^2	4.12×10^{-5}	0.87
0.05	1.59×10^{10}	1.10	9.44×10^7	3.27×10^{37}	0.789	0.211	4.26	1.48	3.22	1.16×10^{-6}	0.88
0.10	2.05	9.76×10^1	8.92	5.80	0.789	0.211	4.26	1.11	1.47	5.67×10^{-8}	0.89
0.15	2.39	8.81	8.48	7.73	0.789	0.211	4.26	9.05×10^3	6.25×10^1		0.89
0.20	2.70	7.93	8.05	9.43	0.789	0.211	4.26	7.58	3.89		0.90
0.30	3.20	6.48	7.27	1.18×10^{38}	0.789	0.211	4.26×10^{-12}	4.97	1.00		0.91
0.40	3.69	5.15	6.50	1.35	0.797	0.203		3.16			0.92
0.50	4.16	3.97	5.77	1.45	0.798	0.202		1.86			0.92
0.60	4.60	3.02	5.12	1.50	0.799	0.201		1.05			0.93
0.70	5.11	2.12	4.43	1.54	0.799	0.201		5.40×10^2			0.93
0.80	5.77	1.25	3.66	1.55	0.800	0.200		1.8			0.94
0.90	6.68	5.78×10^0	2.79	1.56	0.800	0.200					0.94
0.95	9.45	2.76	2.17	1.56	0.800	0.200					0.94
1.00	1.22×10^{11}	7.03×10^{-9}	6.19×10^4	1.56×10^{38}	0.800	0.200					0.63

TABLE VIIb
Hydrogen-depleted model for $M = 20\ M_\odot$ $t = 9.60 \times 10^6$ yr

M_r/M	R cm	ϱ g cm^{-3}	T K	L erg s^{-1}	X_1	X_4	X_{12}	ε_{pp} erg cm^{-1} s^{-1}	ε_{CN} erg g^{-1} s^{-1}	$\varepsilon_{3\alpha}$ erg g^{-1} s^{-1}	β
0.00	0.00	1.86×10^2	1.25×10^8	0.00	0.003	0.997	4.00×10^{-8}	5.57×10^{-1}	2.81×10^5	9.40	0.70
0.05	1.46×10^{10}	1.34	1.09	2.31×10^{38}	0.003	0.997	4.00	3.26	6.34×10^4	9.90×10^{-2}	0.72
0.10	1.92	1.06	9.94×10^7	2.96	0.003	0.997	4.00	2.10	1.80	2.00×10^{-3}	0.73
0.15	2.30	8.37×10^1	9.04	3.16	0.003	0.997	4.00	1.00	2.00×10^3	2.70×10^{-7}	0.74
0.20	2.65	6.54	8.16	3.22	0.003	0.997	4.00×10^{-8}	4.00×10^0	4.87×10^2		0.75
0.30	3.52	2.41	6.54	3.31	0.336	0.664	2.06×10^{-9}	2.60×10^2	4.90		0.77
0.40	4.65	1.07	5.27	3.34	0.653	0.347	2.56×10^{-9}	2.70	2.71		0.79
0.50	6.07	6.09×10^0	4.33	3.35	0.758	0.242		1.15	1.15		0.81
0.60	7.55	3.19	3.47	3.36	0.775	0.225		1.6×10^1			0.83
0.70	9.09	2.22	2.83	3.36	0.788	0.212		1.01×10^0			0.85
0.80	1.10×10^{11}	1.10	2.18	3.37	0.796	0.204					0.86
0.90	1.39	4.25×10^{-1}	1.55	3.37	0.800	0.200					0.87
0.95	1.64	1.81	1.15	3.37	0.800	0.200					0.87
1.00	3.26×10^{11}	1.15×10^{-9}	4.60×10^4	3.37×10^{38}	0.800	0.200					0.41

© Kluwer Academic Publishers • Provided by the NASA Astrophysics Data System

1971Ap&SS..14..399E

up to a mass fraction of about 0.80. The physical parameters of the star at the end of the hydrogen depletion phase are given in Table VIIb. The change of the physical and compositional characteristics with time is illustrated in Figure 6, for the 20 $M_\odot$ star. In the upper figure, the curves L_g/L and L/L_s give, in turn, the variation of the relative contribution of the gravitational energy to the total luminosity and the total luminosity. The scaling factor is $L_s = 10^5\ L_\odot$. ε_{pp}, ε_{CN} and $\varepsilon_{3\alpha}$ represent the variation of the rate of energy generation by the p-p chain, by the CN-cycle and by the triple-alpha reactions, respectively. The scaling factors are $\varepsilon_s = 2.8 \times 10^5$ erg g^{-1} s^{-1} and $\varepsilon_{3\alpha s} = 10^{-3}$ erg g^{-1} s^{-1}. In the lower figure, the change of the central temperature (T_c), the central density (ϱ_c) and the central abundances, by mass of hydrogen (X_1), helium (X_4) and carbon (X_{12}) are shown. The scaling factors are $T_s = 1.25 \times 10^8$ K, $\varrho_c = 186$ g cm^{-3} and $X_{12s} = 4 \times 10^{-8}$.

In the evolution of the 30 $M_\odot$ H-He star, the pure gravitational contraction phase lasts about 1.7×10^5 yr until the central temperature and density reach the values of 8.1×10^7 K and 43 g cm^{-3}. At this stage, the rate of gravitational contraction energy release at the center is 1.36×10^4 erg g^{-1} s^{-1} and the rate of energy generation by the

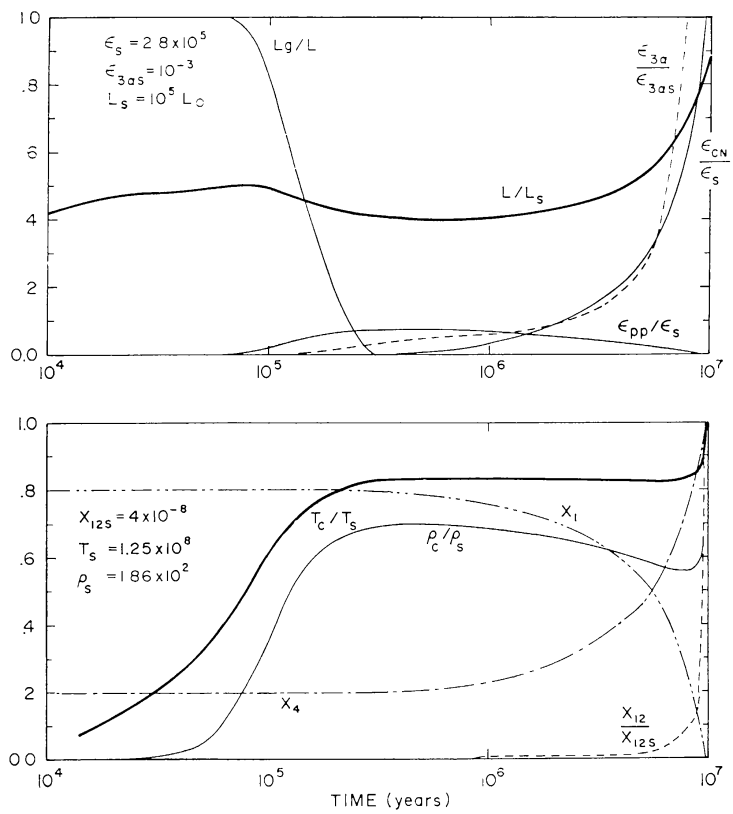

Fig. 6. The variation with time, for a hydrogen-helium star of 20 $M_\odot$, of several quantities. In the lower figure are plotted, the central temperature (T_c), the central density (ϱ_c), and the central abundance, by mass, of hydrogen (X_1), helium (X_4), and carbon (X_{12}). In the upper figure are plotted, the total luminosity (L), the relative contribution of the gravitational energy to the total luminosity (L_g/L), the rate of energy generation by the *p-p* chain (ε_{pp}), by the CN-cycle (ε_{CN}) and by the triple-alpha reactions, at the center of the star. The scaling factors are indicated in the figure.

© Kluwer Academic Publishers • Provided by the NASA Astrophysics Data System

1971Ap&SS..14..399E

p-p chain has the value 4.27×10^3 erg g^{-1} s^{-1}. When gravitational contraction energy supplies half of the total energy output of the star, the central temperature has risen to 1.11×10^8 K, and the density is 102 g cm^{-3}. Thereafter, a sufficient amount of carbon forms by the triple-alpha reaction to make the rate of energy generation from the carbon cycle comparable to that from the p-p chains at the center of the star. The high rate of energy generation by the CN-cycle causes the rapid development of a central convective core, and reduces the total luminosity. It covers about 51% of the total mass of the star when the star reaches the zero-age main-sequence in 2.5×10^5 yr. At this time, one-fourth of the total energy is supplied by the p-p chain reactions, and three-fourths come from the CN-cycle reactions at the center of the star. The physical characteristics of the zero-age main-sequence model are given in Table VIIIa.

During the hydrogen depletion phase, the central temperature slightly decreases even though there is a slow contraction of the central convective core; the large amount of carbon formed at the center of the star is distributed throughout the large convective core, thus reducing the effective amount of carbon in the CN-cycle at the center. The central temperature starts to increase again when the convective core recedes to 0.40 of the total mass. By then, the hydrogen content at the center has dropped to 0.45 and the helium content has increased to 0.55. The p-p chain only contributes 2% of the total nuclear energy at the center of the star. Outside the convective core, the energy generation rate by the p-p chain exceeds the rate by the CN-cycle and extends out to about 80% of the stellar mass.

As the convective core recedes and T_c and ϱ_c keep increasing with increasing μ, the importance of energy generation by the triple-alpha reaction becomes pronounced. When the central helium content has increased to 0.998 at the center of the star, the rate of energy generation by the triple-alpha reactions already exceeds that of the p-p chain reactions inside 7% of the total mass. The physical characteristics of the H-He star of 30 $M_\odot$ are shown in Table VIIIb at the end of the hydrogen depletion phase.

In the evolution of the H-He star of 100 $M_\odot$, more than half of the total pressure is due to the radiation. Therefore, the adiabatic and radiative temperature gradients are very close. The central convective core starts to develop at 5×10^2 yr and it extends to 0.60 of the total mass toward the end of the purely gravitational contraction phase. In the evolution of a normal star of 100 $M_\odot$, the purely gravitational contraction phase ceases when the central temperature and density have reached about 2×10^7 K and 0.2 g cm^{-3}, respectively. By then, the star has contracted to a radius of about 30 $R_\odot$ with a luminosity of about 10^6 $L_\odot$. But the purely gravitational contraction phase of the H-He star of 100 $M_\odot$ lasts until it contracts to a radius of about 5 $R_\odot$ with a corresponding central temperature of 1.26×10^8 K and a density of 41 g cm^{-3}. At first the contribution of nuclear energy to the energy generation is mostly due to p-p chain reactions. The star reaches the zero-age main-sequence in 1.46×10^6 yr with a radius of about 3 $R_\odot$, and a surface temperature of 9.7×10^4 K. At the zero-age main-sequence, the rate of energy generation by the CN-cycle is 1.5×10^5 erg g^{-1} s^{-1} and by the p-p chain the rate is only 4.2×10^3 erg g^{-1} s^{-1}. The central convective core

© Kluwer Academic Publishers • Provided by the NASA Astrophysics Data System

1971Ap&SS..14..399E

TABLE VIIIa

Zero-age main-sequence model for $M = 30\ M_\odot$ $t_{\text{zams}} = 2.50 \times 10^5$ yr

M_r/M	R cm	ϱ g cm^{-3}	T K	L erg s^{-1}	X_1	X_4	X_{12}	ε_{pp} erg cm^{-1} s^{-1}	ε_{CN} erg g^{-1} s^{-1}	$\varepsilon_{3\alpha}$ erg g^{-1} s^{-1}	β
0.00	0.00	1.05×10^2	1.14×10^8	0.00	0.797	0.203	1.33×10^{-10}	2.01×10^4	5.91×10^4	1.07×10^{-3}	0.80
0.05	1.96×10^{10}	8.77×10^1	1.05	1.44×10^{38}	0.797	0.203	1.33	1.45	2.25	4.00×10^{-5}	0.81
0.10	2.50	7.78	9.98×10^7	2.25	0.797	0.203	1.33	1.16	1.17	3.89×10^{-6}	0.82
0.15	2.95	7.00	9.51	2.81	0.797	0.203	1.33	9.56×10^3	6.46×10^3		0.82
0.20	3.33	6.29	9.06	3.20	0.797	0.203	1.33	7.51	3.48		0.83
0.30	3.92	5.42	8.45	3.65	0.797	0.203	1.33	5.38	1.49		0.84
0.40	4.50	4.10	7.48	3.90	0.797	0.203	1.33	3.45	2.8×10^2		0.85
0.50	5.09	3.24	6.66	4.05	0.797	0.203	1.33×10^{-10}	2.21	6.92×10^1		0.86
0.60	5.66	2.47	5.94	4.12	0.800	0.200		1.33			0.87
0.70	6.38	1.65	4.98	4.15	0.800	0.200		5.32×10^2			0.88
0.80	7.08	1.18	4.42	4.16	0.800	0.200		2.56			0.89
0.90	8.16	4.86×10^0	3.20	4.17	0.800	0.200		4.69×10^1			0.89
0.95	9.16	2.18	2.43	4.17	0.800	0.200					0.90
1.00	1.47×10^{11}	7.08×10^{-9}	7.21×10^4	4.17×10^{38}	0.800	0.200					0.52

TABLE VIIIb

Hydrogen-depleted model for $M = 30\ M_\odot$ $t = 6.61 \times 10^6$ yr

M_r/M	R cm	ϱ g cm^{-3}	T K	L erg s^{-1}	X_1	X_4	X_{12}	ε_{pp} erg cm^{-1} s^{-1}	ε_{CN} erg g^{-1} s^{-1}	$\varepsilon_{3\alpha}$ erg g^{-1} s^{-1}	β
0.00	0.00	1.41×10^2	1.33×10^8	0.00	0.002	0.998	8.36×10^{-8}	1.56×10^{-1}	4.42×10^5	3.30×10^1	0.60
0.05	1.82×10^{10}	1.02	1.17	5.87×10^{38}	0.002	0.998	8.36	9.08×10^{-2}	1.02	3.54×10^{-1}	0.61
0.10	2.41	8.12×10^1	1.08	7.75	0.002	0.998	8.36	6.15	3.45×10^4	1.00×10^{-2}	0.62
0.15	2.87	6.53	9.91×10^7	8.43	0.002	0.998	8.36	4.23	1.20	2.53×10^{-4}	0.62
0.20	3.32	5.14	9.04	8.71	0.002	0.998	8.36×10^{-8}	2.78×10^0	3.63×10^3	3.01×10^{-6}	0.63
0.30	4.18	2.69	7.39	8.90	0.074	0.926	1.52×10^{-8}	1.91×10^1	1.70		0.65
0.40	5.62	8.58×10^0	5.82	9.00	0.506	0.494	2.02×10^{-9}	1.64×10^2	2.83×10^1		0.66
0.50	7.39	4.90	4.67	9.05	0.628	0.272	1.12×10^{-10}	9.66×10^1 —	9.67×10^{-1}		0.69
0.60	9.57	2.21	3.70	9.08	0.749	0.251		2.88	2.78×10^{-3}		0.71
0.70	1.19×10^{11}	1.22	2.96	9.10	0.793	0.207		8.68×10^0			0.73
0.80	1.48	6.33×10^{-1}	2.30	9.11	0.797	0.203		1.44			0.75
0.90	1.95	2.12	1.55	9.12	0.800	0.200					0.76
0.95	2.36	7.90×10^{-2}	1.10	9.13	0.800	0.200					0.77
1.00	4.88×10^{11}	5.58×10^{-10}	4.82×10^4	9.13×10^{38}	0.800	0.200					0.22

© Kluwer Academic Publishers • Provided by the NASA Astrophysics Data System

1971Ap&SS..14..399E

extends to a fractional mass of 0.72. The physical characteristics of the zero-age main-sequence model for the H-He star of 100 $M_\odot$ are given in Table IXa.

One interesting point concerning the evolution is the occurence of a density inversion in the central part of the star. The high radiation pressure provides most of the pressure balance up to 20% of the star's mass. The highest interior density is not the central one, but the one corresponding to a fractional mass 0.20. From this point outward, the gas pressure becomes the main contributor to the total pressure and the density distribution is governed by the gas pressure. During the hydrogen depletion phase, the central temperature stays near 1.2×10^8 K, enabling the CN-cycle to operate with the continuous formation of C^{12} from the 3α-reaction.

Once the central hydrogen content is sufficiently depleted and the central convective core has receded to 40% of the stellar mass, the central temperature starts to increase. This increases the ratio of the radiation pressure to the total pressure, since $P_r \sim T^4$ and $P_g \sim T\varrho$. Therefore, the highest interior density is 3.18 g cm^{-3} at the point corresponding to the fractional mass 0.20. The physical characteristics of the star at the end of the hydrogen depletion phase are given in Table IXb.

The evolutionary trend of H-He stars of 200 $M_\odot$ is similar to that of the 100 $M_\odot$ star. But, due to the larger radiation pressure, the convective region extends to a larger fractional mass of 0.80 when the star reaches the zero-age main sequence in 1.71×10^5 yr. The peak of the interior density is at the fractional mass 0.30. The purely gravitational contraction phase lasts about 6×10^4 yr until the central temperature and density attain the values of 1.41×10^8 K and 37 g cm^{-3}, respectively. By the end of the purely gravitational contraction phase, the fractional amount of C^{12} is 4.6×10^{-12}. The sudden increase of the rate of energy generation from the CN-cycle extends the boundary of the convective core up to a fractional mass of 0.80, reducing the central temperature to 1.28×10^8 K and density to 11.9 g cm^{-3}. During the main-sequence evolution, hydrogen depletion will continue mainly through the CN-cycle.

The evolution of H-He stars of 200 $M_\odot$ was followed until the central hydrogen content dropped to 0.38. As the luminosity increases during the main-sequence evolution, the radiation pressure becomes a large fraction of the total pressure throughout the star. In Tables Xa and Xb, the physical characteristics of the H-He star of 200 $M_\odot$ have been summarized for the zero-age main-sequence model and for the last computed model, respectively.

The last computed model of the star, with a central hydrogen content of 0.38, has a total luminosity $L = 1.39 \times 10^{40}$ erg s^{-1}, and a radius $R = 4.25 \times 10^{11}$ cm. Consider the radiation emitted from the surface of the star at this time. The radiative flux will transfer momentum to a gram of material in the surface layers at a rate $(\kappa/c)\,(L/4\pi R^2)$. At the high temperatures under consideration, the opacity κ of the surface material will be primarily due to electron scattering, and hence the above expression amounts to 6.96×10^4 dyn per gram. The gravitational force exerted on a gram of material at the surface of the star is $(GM)/R^2 \sim 1.46 \times 10^5$ dyn per gram. It may be seen that the radiation pressure is nearly able to expel material from the surface of the star. Since the luminosity of the star has been increasing substantially throughout its main-

© Kluwer Academic Publishers • Provided by the NASA Astrophysics Data System

1971Ap&SS..14..399E

TABLE IXa

Zero-age Main-sequence model for $M = 100\ M_\odot$ $t_{\text{zams}} = 1.46 \times 10^5$ yr

M_r/M	R cm	ϱ g cm^{-3}	T K	L erg s^{-1}	X_1	X_4	X_{12}	ε_{pp} erg cm^{-1} s^{-1}	ε_{CN} erg g^{-1} s^{-1}	$\varepsilon_{3\alpha}$ erg g^{-1} s^{-1}	β
0.00	0.00	1.88×10^1	1.25×10^8	0.00	0.790	0.210	7.71×10^{-10}	4.18×10^3	1.47×10^5	8.60×10^{-4}	0.36
0.05	4.96×10^{10}	2.04	1.18	1.07×10^{39}	0.790	0.210	7.71	4.06	8.92×10^4	1.36	0.41
0.10	6.16	2.19	1.12	1.85	0.790	0.210	7.71	3.99	5.95	2.80×10^{-5}	0.47
0.15	6.97	2.28	1.07	2.34	0.790	0.210	7.71	3.81	3.94	5.69×10^{-6}	0.52
0.20	7.62	2.31	1.02	2.68	0.790	0.210	7.71	3.56	2.56	1.05	0.55
0.30	8.67	2.24	9.37×10^7	3.08	0.790	0.210	7.71	2.92	1.01	2.64×10^{-8}	0.61
0.40	9.54	2.06	8.59	3.25	0.790	0.210	7.71	2.16	3.39×10^3		0.65
0.50	1.04×10^{11}	1.79	7.84	3.35	0.790	0.210	7.71	1.60	1.20		0.68
0.60	1.12	1.46	7.03	3.40	0.790	0.210	7.71	1.00	2.80×10^2		0.71
0.70	1.21	1.10	6.24	3.45	0.790	0.210	7.71×10^{-10}	5.90×10^2	5.10×10^1		0.72
0.80	1.32	7.18×10^0	5.30	3.48	0.800	0.200		2.80			0.73
0.90	1.47	3.62	4.14	3.51	0.800	0.200					0.74
0.95	1.56	2.33	3.56	3.52	0.800	0.200					0.75
1.00	2.35×10^{11}	5.12×10^{-9}	9.74×10^4	3.53×10^{39}	0.800	0.200					0.24

TABLE IXb

Hydrogen-depleted model for $M = 100\ M_\odot$ $t = 3.64 \times 10^6$ yr

M_r/M	R cm	ϱ g cm^{-3}	T K	L erg s^{-1}	X_1	X_4	X_{12}	ε_{pp} erg cm^{-1} s^{-1}	ε_{CN} erg g^{-1} s^{-1}	$\varepsilon_{3\alpha}$ erg g^{-1} s^{-1}	β
0.00	0.00	2.15×10^1	1.36×10^8	0.00	0.007	0.993	6.52×10^{-8}	4.1×10^{-1}	2.6×10^5	1.5×10^0	0.18
0.05	4.70×10^{10}	2.49	1.28	2.11×10^{39}	0.007	0.993	6.52	4.3	1.8	3.8×10^{-1}	0.23
0.10	5.77	2.85	1.22	3.66	0.007	0.993	6.52	4.6	1.4	1.3	0.28
0.15	6.47	3.09	1.17	4.76	0.007	0.993	6.52	4.5	9.4×10^4	2.8×10^{-2}	0.32
0.20	7.02	3.18	1.11	5.52	0.007	0.993	6.52	4.3	6.0	5.3×10^{-3}	0.36
0.30	7.94	2.96	1.00	6.28	0.007	0.993	6.52×10^{-8}	3.3	2.1	9.0×10^{-5}	0.42
0.40	8.80	2.18	9.00×10^7	6.52	0.030	0.970	3.57×10^{-8}	4.2×10^0	1.2	4.3×10^{-7}	0.44
0.50	1.00×10^{11}	1.04	7.84	6.66	0.280	0.720	7.75×10^{-9}	1.1×10^2	2.4×10^3		0.44
0.60	1.18	4.53×10^0	6.64	6.66	0.680	0.320	1.58×10^{-9}	2.1	7.8×10^1		0.45
0.70	1.44	2.76	5.37	6.65	0.680	0.320		7.8×10^1	3.5×10^0		0.48
0.80	1.77	1.30	4.20	6.64	0.760	0.240		2.5	2.2×10^{-2}		0.49
0.90	2.24	4.80×10^{-1}	2.97	6.62	0.800	0.200		3.5×10^0			0.51
0.95	2.65	2.03	2.20	6.62	0.800	0.200					0.52
1.00	5.39×10^{11}	9.16×10^{-11}	7.52×10^4	6.62×10^{39}	0.800	0.200					0.01

© Kluwer Academic Publishers • Provided by the NASA Astrophysics Data System

1971Ap&SS..14..399E

TABLE Xa

Zero-age main-sequence model for $M = 200\ M_\odot$ $t_{\text{zams}} = 1.71 \times 10^5$ yr

M_r/M	R cm	ϱ g cm^{-3}	T K	L erg s^{-1}	X_1	X_4	X_{12}	ε_{pp} erg cm^{-1} s^{-1}	ε_{CN} erg g^{-1} s^{-1}	$\varepsilon_{3\alpha}$ erg g^{-1} s^{-1}	β
0.00	0.00	1.19×10^1	1.28×10^8	0.00	0.780	0.220	1.13×10^{-9}	2.67×10^3	1.65×10^5	7.79×10^{-4}	0.24
0.05	7.30×10^{10}	1.25	1.22	2.67×10^{39}	0.780	0.220	1.13	2.61	1.14	2.10	0.28
0.10	9.11	1.36	1.18	4.54	0.780	0.220	1.13	2.64	8.75×10^4	7.36×10^{-5}	0.32
0.15	1.03×10^{11}	1.45	1.14	6.03	0.780	0.220	1.13	2.66	6.63	6.78×10^{-6}	0.36
0.20	1.12	1.53	1.09	7.22	0.780	0.220	1.13	2.61	4.79	4.28×10^{-7}	0.40
0.30	1.26	1.59	1.02	8.66	0.780	0.220	1.13	2.36	2.37	1.28×10^{-8}	0.46
0.40	1.38	1.54	9.35×10^7	9.41	0.780	0.220	1.13	1.95	9.81×10^3		0.52
0.50	1.48	1.41	8.64	9.73	0.780	0.220	1.13	1.48	3.80		0.55
0.60	1.58	1.21	7.82	9.89	0.780	0.220	1.13	1.00	1.20		0.59
0.70	1.69	9.63×10^0	7.00	9.96	0.780	0.220	1.13	6.64×10^2	2.52×10^2		0.61
0.80	1.81	6.71	6.09	1.00×10^{40}	0.780	0.220	1.13×10^{-9}	3.34	3.27×10^1		0.63
0.90	2.00	3.36	4.75	1.00	0.800	0.200		9.78×10^1			0.64
0.95	2.15	1.78	3.81	1.00	0.800	0.200					0.65
1.00	3.01×10^{11}	2.92×10^{-9}	1.12×10^5	1.00×10^{40}	0.800	0.200					0.11

TABLE Xb

Hydrogen-depleted model for $M = 200\ M_\odot$ $t = 1.96 \times 10^6$ yr

M_r/M	R cm	ϱ g cm^{-3}	T K	L erg s^{-1}	X_1	X_4	X_{12}	ε_{pp} erg cm^{-1} s^{-1}	ε_{CN} erg g^{-1} s^{-1}	$\varepsilon_{3\alpha}$ erg g^{-1} s^{-1}	β
0.00	0.00	9.13×10^0	1.21×10^8	0.00	0.380	0.620	6.52×10^{-9}	4.32×10^2	2.12×10^5	1.94×10^{-3}	0.17
0.05	7.94×10^{10}	9.87	1.16	3.35×10^{39}	0.380	0.620	6.52	4.35	1.56	5.94×10^{-4}	0.20
0.10	9.87	1.10×10^1	1.12	6.08	0.380	0.620	6.52	4.57	1.27	2.33	0.24
0.15	1.11×10^{11}	1.22	1.09	8.23	0.380	0.620	6.52	4.75	1.01	8.49×10^{-5}	0.27
0.20	1.21	1.31	1.05	1.00×10^{40}	0.380	0.620	6.52	4.79	7.60×10^4	2.52	0.31
0.30	1.35	1.40	9.77×10^7	1.22	0.380	0.620	6.52	4.46	3.92	1.64×10^{-6}	0.38
0.40	1.46	1.36	9.00	1.33	0.380	0.620	6.52	3.69	1.62	4.40×10^{-8}	0.43
0.50	1.56	1.22	8.31	1.37	0.380	0.620	6.52	2.80	6.10×10^3		0.46
0.60	1.68	9.60×10^0	7.51	1.39	0.380	0.620	6.52×10^{-9}	1.91	1.80		0.48
0.70	1.70	9.07	7.41	1.39	0.390	0.610	6.28×10^{-9}	1.79	1.25		0.48
0.80	1.76	6.37	7.01	1.39	0.600	0.400	2.89	2.85	3.76×10^2		0.48
0.90	1.94	4.12	6.03	1.39	0.640	0.360	2.45	1.37	3.27×10^1		0.49
0.95	2.10	2.64	5.26	1.39	0.720	0.280	1.32	8.08×10^1	2.27×10^0		0.50
1.00	4.25×10^{11}	3.90×10^{-12}	1.02×10^5	1.39×10^{40}	0.800	0.200					0.0002

© Kluwer Academic Publishers • Provided by the NASA Astrophysics Data System

1971Ap&SS..14..399E

sequence evolution, it is evident that the evolutionary study cannot be carried further than that indicated above, since the radiation pressure will shortly cause loss of mass from the surface, which would have to be taken into account in the evolution. Since this refinement has not be attempted in the present study, the evolutionary calculations were terminated at this point. It is evident that this radiative expulsion of mass would even more rapidly become a dominating feature of the evolution of still more massive hydrogen-helium stars.

6. Discussion

The most important difference between the hydrogen-helium stars and normal stars is the much higher surface temperature of the former. This temperature lies in the vicinity of 10^5 K for the massive stars which have been studied.

If massive hydrogen-helium stars are formed in the early stages of galaxy formation, then their luminosity will be extremely high, and the color temperature of the radiation will also be extremely high. The problem of the detection of extremely luminous young galaxies has been discussed by Partridge and Peebles (1967). Their motivation was the seeming requirement to manufacture large amounts of helium from hydrogen in the early stages of galactic evolution. This requirement is not present in the chemical evolution studies of Truran and Cameron (1971), but nevertheless the latter authors require a great deal of mass to participate in the first stellar generation, leading to formation of a very large number of massive black holes. In any case, the current calculations seem quite relevant to a discussion of the observability of very young galaxies or star clusters.

If these were generally formed at about one-tenth of the present age of the universe, as proposed by Partridge and Peebles (1967), then the radiation with a color temperature of the order 10^5 K which would be emitted from them would have been subjected to a redshift of a factor 10, bringing the color temperature down to 10^4 K at the present time. Such objects may not be easy to distinguish from current galaxies on the basis of color temperature; they would certainly not emit strongly in the infrared as suggested by Partridge and Peebles. If the objects are formed at a still later stage, perhaps one-third of the present age of the universe, then the present color temperature of the radiation from them would be of the order of 3×10^4 K. They would appear as extremely blue objects, and it is interesting to speculate that the very large number of blue stellar objects, some of which are quasars, may include clusters containing the first generation of hydrogen-helium stars. A further investigation of this suggestion would require a much more extensive spectroscopic study of faint blue objects.

Acknowledgements

This research has been supported in part by grants from the National Science Foundation and the National Aeronautics and Space Administration. We thank Mr M. Pine for extensive programming assistance with the calculations.

© Kluwer Academic Publishers • Provided by the NASA Astrophysics Data System

1971Ap&SS..14..399E

References

Ezer, D.: 1961, *Astrophys. J.* **133**, 159.
Ezer, D. and Cameron, A. G. W.: 1967, *Can. J. Phys.* **45**, 3429.
Ezer, D. and Cameron, A. G. W.: 1971, *Astrophys. Space Sci.* **10**, 52.
Iben, I.: 1965, *Astrophys. J.* **141**, 993.
Partridge, R. B. and Peebles, P. J. E.: 1967, *Astrophys. J.* **148**, 377.
Reeves, H.: 1965, in *Stars and Stellar Systems* (ed. by L. H. Aller and D. B. McLaughlin), Vol. VIII, University of Chicago Press, Chicago.
Schmidt, M.: 1963, *Astrophys. J.* **137**, 758.
Truran, J. W. and Cameron, A. G. W.: 1971, to be published.

© Kluwer Academic Publishers • Provided by the NASA Astrophysics Data System